Hindawi
Journal of Nanotechnology
Volume 2017, Article ID 7607658, 9 pages
https://doi.org/10.1155/2017/7607658

Research Article

Magnetic Cobalt and Cobalt Oxide Nanoparticles in Hyperbranched Polyester Polyol Matrix

O. I. Medvedeva, S. S. Kambulova, O. V. Bondar, A. R. Gataulina, N. A. Ulakhovich, A. V. Gerasimov, V. G. Evtugyn, I. F. Gilmutdinov, and M. P. Kutyreva

Department of Inorganic Chemistry, Kazan Federal University, 18 Kremlyovskaya St., Kazan 420008, Russia

Correspondence should be addressed to M. P. Kutyreva; mkutyreva@mail.ru

Received 28 May 2017; Accepted 16 July 2017; Published 20 August 2017

Academic Editor: Enkeleda Dervishi

A series of cobalt (Co) and its oxides based nanoparticles were synthesized by using hyperbranched polyester polyol Boltorn H20 as a platform and sodium borohydride as a reducing agent. UV, FT-IR, XRD, NTA, and TEM methods were employed to obtain physicochemical characteristics of the products. The average diameter of Co nanoparticles was approximately 8.2 ± 3.4 nm. Their magnetic properties, including hysteresis loop, field-cooled, and zero field-cooled curves were investigated. The nanoparticles exhibit superparamagnetism at room temperature, accompanied by magnetic hysteresis below the blocking temperature.

1. Introduction

Magnetic nanoparticles exhibit specific physical properties and are of great interest because of their prospective applications in biology and medicine [1–5] for magnetic cell separation [6], magnetically controlled delivery of anticancer drugs [7, 8], magnetic resonance imaging (MRI) contrast enhancement [9, 10], and hypothermia treatment [11]. Most of these applications require chemically stable, well-dispersed, and uniform sized particles.

The magnetic properties of nanoparticles are determined by many factors. The chemical composition, crystal structure and the degree of its defectiveness, morphology, and the interaction of particles with the surrounding matrix and neighboring particles play crucial role [12, 13]. It is possible to control the magnetic characteristics of materials by changing the morphology of such nanoparticles [12]. Among numerous magnetic nanomaterials, cobalt (Co) and its oxides based nanoparticles have attracted particular attention because of their excellent optical [14, 15], magnetic [12, 13, 16], and catalytic properties [17, 18]. For the synthesis of such compounds, the most common methods are solvent-thermal [19–21], thermolysis of the carbonyl [22] or other cobalt complexes [23], and chemical reduction of cobalt salts [24, 25].

The strong magnetic interaction between cobalt nanoparticles and their propensity for oxidation make it difficult to obtain stable colloids. Therefore, in most cases, organic stabilizers are used to control the growth of nanoparticles and prevent the occurrence of adverse reactions [1, 26].

The nature of the stabilizer often determines the morphology of nanoparticles and the properties of the hybrid material. The use of polymer matrix for stabilization makes it possible to combine the unique properties of metal nanoparticles with useful properties of polymers [1]. The molecules of dendrimers and hyperbranched polymers (HBPs) with core-shell structure in comparison with linear polymers have a number of advantages [27–30]. They have a three-dimensional structure, large number of heteroatoms, functional groups, and cavities [31, 32].

Usage of HBP as a platform for cluster growth, both cluster stability and full control over size, and size distribution were achieved by simultaneously allowing access of substrates to the cluster surface. An additional advantage of HBP matrix in the synthesis of practically useful metal nanoparticles is their biosimilar topological structure and simplicity of synthesis [33, 34]. Earlier it was shown by some authors how series of magnetic cobalt (Co) nanoparticles could be stabilized by a poly-amidoamine (PAMAM) dendrimer [28], polyamine dendrimers with a trimesyl core [29], and

hydroxyl-terminated PAMAM dendrimers [30]. PAMAM is a highly branched macromolecule, which contains interior tertiary amine groups which can effectively coordinate metal ions. Such metal ions may then be reduced to the encapsulated metal particles that are highly stable in solution. Since the same number of chelating sites is present in all dendrimer molecules, this process can yield to monodisperse metal particles [28]. However, the presence of primary amines results in a high cytotoxicity for many cellular systems [35]. Therefore, for the purposes of cell sorting, medical diagnosis, and controlled drug delivery, the strategy for the synthesis of magnetic cobalt nanoparticles is based on the use of nontoxic, biosimilar, and biodegradable hyperbranched polymers and dendrimers. Such compounds include hyperbranched polyester polyols (HBPO) of various generations [36].

In this study, we describe the synthesis of Co nanoparticles via the matrix of nontoxic hyperbranched polyester polyol based on 2,2-bis-hydroxymethyl-propionic acid.

2. Materials and Methods

2.1. Materials. The initial reagent was anhydrous salt cobalt (II) chloride ($CoCl_2$) (97%, Alfa Aesar). Stabilizer was hyperbranched polyester polyol Boltorn H20 (BH20) (Sigma-Aldrich, theoretically having 16 hydroxyl end groups per molecule and the average molecular weight of 1749 g/mol). Sodium borohydride $NaBH_4$ (98%, Alfa Aesar) was used as a reducing agent. The organic solvents such as ethanol and diethyl ether were used as solvents for the synthesis and isolation of nanoparticles.

2.2. Characterization. The electronic absorption spectra were recorded on Lambda 750 (Perkin Elmer) in the wavelength range from 200 to 1000 nm at $T = 25 \pm 0.01$ C, using a temperature-maintaining system including a cell holder flow thermostat «Julabo MB-5A» and a Peltier PTP-1 thermostat. Quartz cells with a thickness of 1 cm were used for the measurements. The measurement accuracy for absorbance (A) was ±1%.

The size, concentration, and movement of nanoparticles were determined using the NanoSight LM-10 (Malvern Instruments Ltd, UK) equipped with a CMOS camera C11440-50B with scientific image sensor FL-280 Hamamatsu Photonics (Japan) as a detector. Measurements were carried out in a special cell for organic solvents having a modified entry angle for the laser beam into the solution, a 405 nm laser (version cd, S/N 2990491), and Kalrez sealing ring. Contact thermometer OMEGA HH804 (Engineering, Inc/Stamford, CT, USA) was used to determine the temperature in the cell during the experiment. The NanoSight NTA 2.3 software (build 0033) was used to process the results.

ATR-FT-IR spectra were recorded over the range from 4000 to 400 cm^{-1} using a FT-IR spectrometer Spectrum 400 (Perkin Elmer) with a universal ATR accessory and a ZnSe prism. The resolution of the spectra was 1 cm^{-1} and scanning was repeated 16 times.

X-ray powder diffraction (XRPD) studies of nanoparticles samples were made using a MiniFlex 600 diffractometer (Rigaku, Japan) equipped with a D/teX Ultra detector. In this experiment, Cu Kα radiation (40 kV, 15 mA) was used and data was collected at room temperature in the range of 2θ from 3 to 100° with a step of 0.02° and exposure time at each point of 0.24 s without sample rotation.

Magnetic properties were measured by PPMS-9 (Quantum Design, USA) equipped with vibrating sample magnetometer (VSM). Zero field-cooled (ZFC) and field-cooled (FC) measurements were performed in 100 Oe. Field dependencies of magnetization were measured at 5–300 K at field range from −1 T to 1 T.

Analysis of samples was carried out in a transmission electron microscope Hitachi HT7700 Exalens. Sample preparation was as follows: 10 microliters of the suspension was placed on a formvar/carbon lacey 3 mm copper grid, and drying was performed at room temperature. After drying grid was placed in a transmission electron microscope using special holder for microanalysis. Analysis was held at an accelerating voltage of 100 kV in TEM mode, and the elemental analysis was carried out in STEM mode, at the same parameters using Oxford Instruments X-Max™ 80 T detector. The size and shape of hybrid NPs were estimated via AxioVision rel.48 soft.

The size distribution of cobalt nanoparticles was obtained by TEM images processing using AxioVision program, version 4.8.2. The size distribution curve was constructed on the base of fivefold sampling of 400 treated nanoparticles.

*2.3. The Synthesis of Co Nanoparticles Stabilized by HBP*O. HBPO BH20 was dissolved in 30 ml of 50% water-ethanol solution ($c_{HBPO} = 0.1$ mM); then 10 ml of $CoCl_2$, dissolved in deionized water, was added. The molar ratio of Co^{2+} to HBPO was 4 : 1, 8 : 1, 10 : 1, 12 : 1, and 16 : 1. The solution was stirred for 12 hours and then was cooled to 4°C. After that 10 mL of 0.3 mol × L^{-1} $NaBH_4$ solution was added dropwise with constant stirring. The solid was separated and washed 2 times: by deionized water first, then by ethyl alcohol, dried under vacuum without heating.

3. Results and Discussion

Synthesis of organic-inorganic nanocomposites was carried out in the following way: the first stage is the formation of complex forms of Co^{2+}, HBPO; the second stage was the synthesis of polymer-metal nanocomposites by the chemical reduction method [37].

HBPO BH20 was used to stabilize cobalt nanoparticles. The molecule of HBPO BH20 contains ester and hydroxyl groups (Figure 1). Molecules of hyperbranched polymers of low generation ($G = 2$), as well as dendrimer molecules of low generation, exist in a relatively open structure [34]. The stage of metal ions organization on a polymer matrix can determine the morphology of organic-inorganic nanomaterial; therefore, at the first stage of the work, the interaction of Co^{2+} ions with a polymer platform of HBPO was studied. Features of the HBPO structure suggest the associates formation in solution due to intermolecular and intramolecular hydrogen bonds [34]. The NTA method showed that in BH20 solution with a concentration of 8.7×10^{-5} mg/ml there were two types

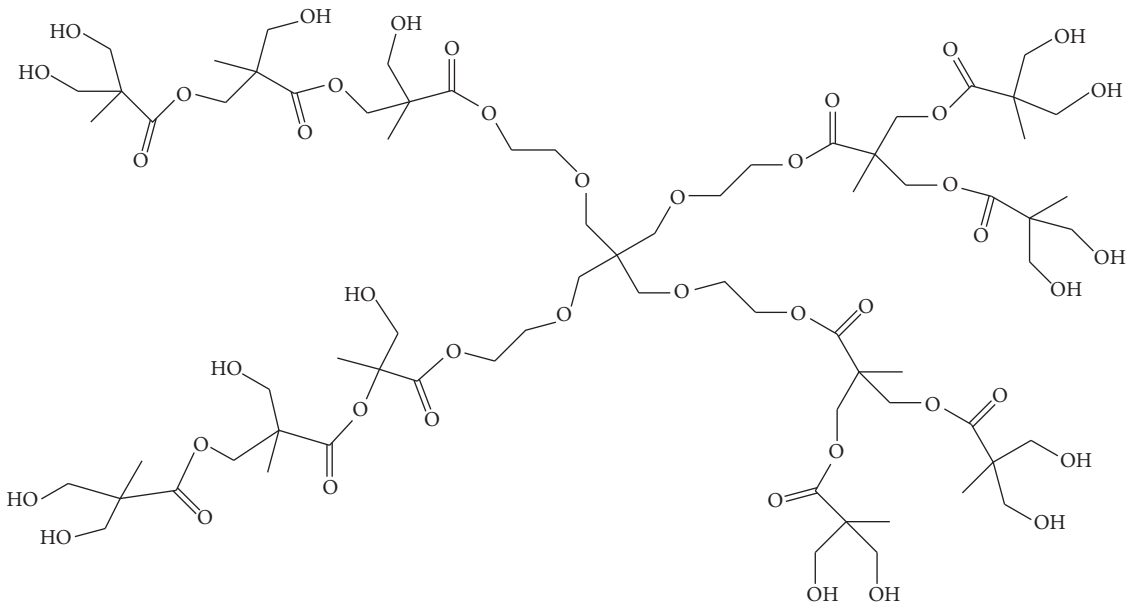

Figure 1: Structure of HBPO G2.0 (BH20).

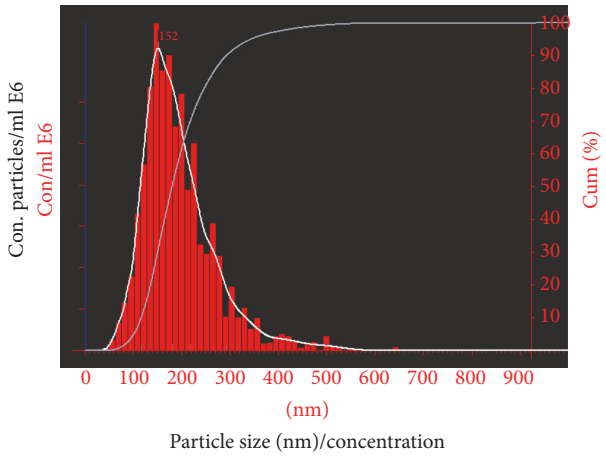

Figure 2: Concentration and size distribution from NTA measurements of BH20 aqueous solution.

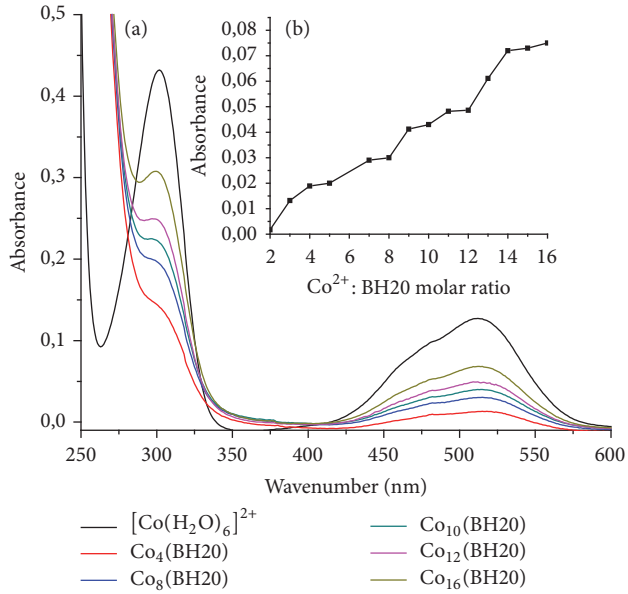

Figure 3: (a) UV-vis absorption spectra of Co^{2+}-BH20 complex with different Co^{2+} : BH20 molar ratio in aqueous solution. (b) Spectrophotometric titration solution of BH20 by $CoCl_2$ solution (c_{BH20} = 0.1 mM, c_{CoCl2} = 0.1–1.6 mM, and λ = 518 nm) (b).

of closely related associates with a hydrodynamic diameter of 150 ± 8 nm (Figure 2).

In the absorption spectra of the HBPO BH20 solution, there were no absorption bands in the visible region of the spectrum (Figure 3). In the absorption spectrum of the aqueous solution of cobalt chloride, there was an intense absorption band in the region of 510 nm due to the d-d transitions of 4T1 g (F) → 4T1 g (P) in the $[Co(H_2O)_6]^{2+}$ aqua ions. Absorption at 290 nm was assigned to charge transfer from the nonbonding orbital of chloride ions to half-filled d-orbitals of cobalt (II) [38]. In solutions of $CoCl_2$: BH20 at different molar ratios of c_{co2+}/c_{BH20} from 4 : 1 to 16 : 1, the absorption bands intensity and the shift of the maxima to 518 nm were observed for both absorption bands, which corresponds to the interaction of Co^{2+} ions with the terminal hydroxyl groups of HBPO and the formation of Co^{2+}, BH20. Spectrophotometric titration plot (Figure 3(b)): absorbance at the maximum of 518 nm 5 levels was observed, according to the formation of the five main complex forms (Table 1).

NTA analysis showed that the increase in the molar ratio c_{co2+}/c_{BH20} in aqua solution from 4 : 1 to 16 : 1 leads to the increase of hydrodynamic diameter of

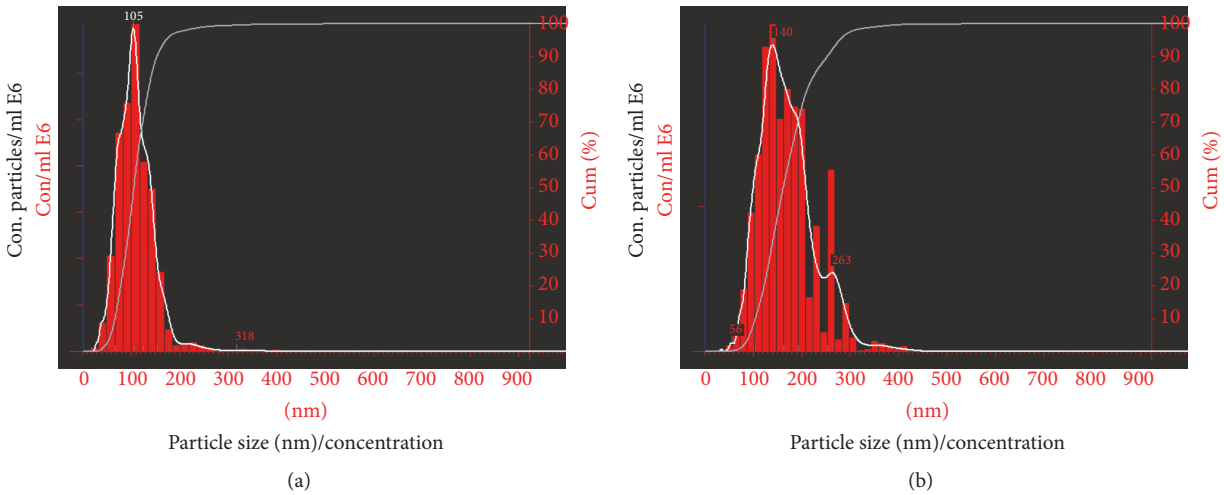

Figure 4: Concentration and size distribution from NTA measurements of complexes Co_8(BH20) (a) and Co_{10}(BH20) (b) in aqueous solution.

Table 1: Stability constants (lgβ), hydrodynamic diameter (d_h), and concentration of complexes Co_n(BH20) in aqueous solution.

Complex	lg β	d_h, nm
Co_4(BH20)	6.2	96 ± 17
Co_8(BH20)	10.4	105 ± 10
Co_{10}(BH20)	17.7	140 ± 18 263 ± 10
Co_{12}(BH20)	26.2	123 ± 15 168 ± 20
Co_{16}(BH20)	31.1	74 ± 5 124 ± 10 210 ± 17

associates from 96 ± 17 nm to 210 ± 17 nm and their polydispersity (Table 1, Figure 4, Supplementary Figures S1, S2; see Supplementary Material available online at https://doi.org/10.1155/2017/7607658).

It can be assumed that the introduction of cobalt ions into the BH20 solution leads to a violation of the hydrogen bonding system, followed by the destruction of the BH20 associates and the formation of associates of complex forms Co_n(BH20) (n = 4, 8, and 10) of smaller size.

Comparing the data of UV-vis spectroscopy and NTA analysis, it can be assumed that an increase in the molar ratio Co^{2+} : BH20 from 4 : 1 to 16 : 1 leads to a decrease in the proportion of coordinated hydroxylic groups of HBPO in the inner sphere of the Co^{2+} ion that could be indicated by a decrease in the "red shift" value and an increase in the hydrodynamic diameter of Co_n(BH20) associates.

Synthesis of cobalt nanoparticles (CoNPs) was carried out by the reduction of Co_n(BH20) complex forms (n = 4, 8, 10, 12, and 16) by sodium borohydride:

$$2Co^{2+} + BH_4^- + 4OH^- \longrightarrow 2Co^{\bullet 0} + 3B(OH)_4^- + 2H_2 \quad (1)$$

During the reduction process, for all ratios, the color of the solution has changed from light pink (Figures 5(a) and 5(d)) to black (Figures 5(b) and 5(e)).

After the reduction of all complex forms according to the UV/vis spectroscopy data, the absorption bands disappear at λ = 510 nm and 302 nm, characteristic for aqua ions $[Co(H_2O)_6]^{2+}$. During the reduction of Co_8(BH20) and Co_{10}(BH20) forms, a weak absorption peak of the PPR in the region of 260 nm appeared (Figure 6). After the reduction of Co_{12}(BH20), an absorption maximum appears in the region of 274 nm, characteristic of cobalt nanoparticles Co^0 [30, 39, 40]. After the reduction of Co_{16}(BH20) complex form, CoNPs have appeared, which had two maxima in the region of 268 nm and 385 nm, characteristic for nanoparticles Co_3O_4 [41, 42].

CoNPs (Co^{2+} : HBPO = 4 : 1, 8 : 1, and 10 : 1) samples failed to isolate quantitively. CoNPs (Co^{2+} : HBPO = 12 : 1 and 16 : 1) samples were isolated from the solution as the black powder. However, CoNPs (16 : 1) have possessed less stability and were easily oxidized by air oxygen, and the color of the powder changed to green, indicating the presence of CoO.

The FR-IR spectra of BH20, CoNPs (12 : 1) and CoNPs (16 : 1) solids (oxidized forms), were shown in Figure 7. It was found that, during the synthesis of CoNPs nanocomposites (12 : 1), the polymer matrix of HBPO did not degrade and did not undergo significant changes. The peaks at 3356 cm^{-1} belong to H-bonded OH, 2945 cm^{-1} and 2859 cm^{-1} ascribed to antisymmetric and symmetric C–H, 1728 cm^{-1} ascribed to H-bonded carbonyl (ν_{bonded}C=O), 1440 cm^{-1} symmetric COO-stretching, 1400 cm^{-1} and 1375 cm^{-1} CH_2 deformation antisymmetric and symmetric, 1305 cm^{-1} deformation H-bonded, 1220 cm^{-1} and 1120 cm^{-1} C-O and O-C stretching ester, and 1040 cm^{-1} CO(-OH) stretching hydroxyl in BH20 [34]. At FR-IR spectra CoNPs (12 : 1) and CoNPs (16 : 1) a band at 1645 cm^{-1} appeared, which could be associated with the formation and crystallization of a by-product $NaBO_3$ in cavities of HBPO [43]. An increase in the absorption intensity

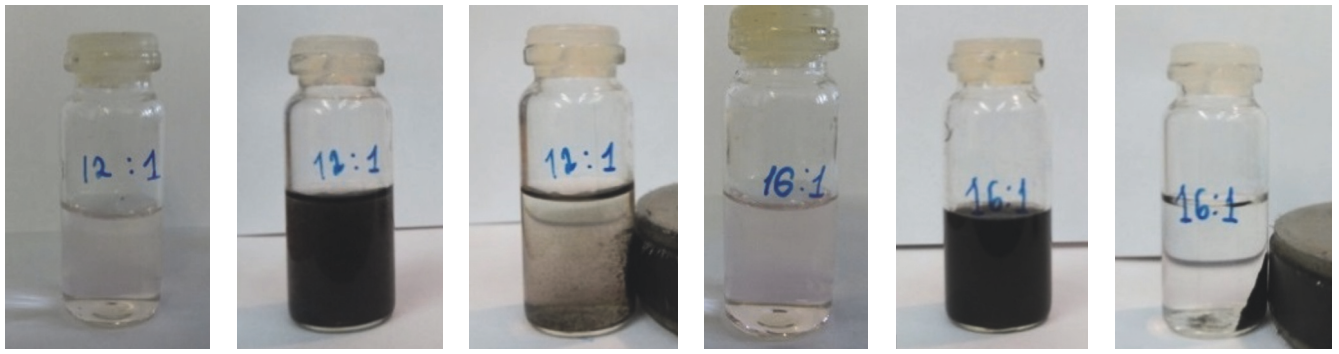

Figure 5: Color transformation of Co^{2+}-BH20 solution before (a, d) and after (b, e) reduction; the collection of CoNPs by a magnet (c, f).

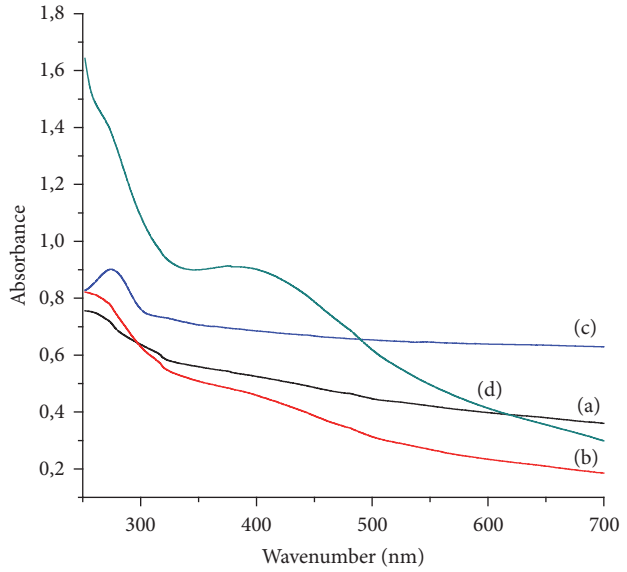

Figure 6: UV/vis spectra of aqueous solutions containing CoNPs after Co_8(BH20) reduction (a), CoNPs after Co_{10}(BH20) reduction (b), CoNPs after Co_{12}(BH20) reduction (c), and CoNPs after Co_{16}(BH20) reduction (d).

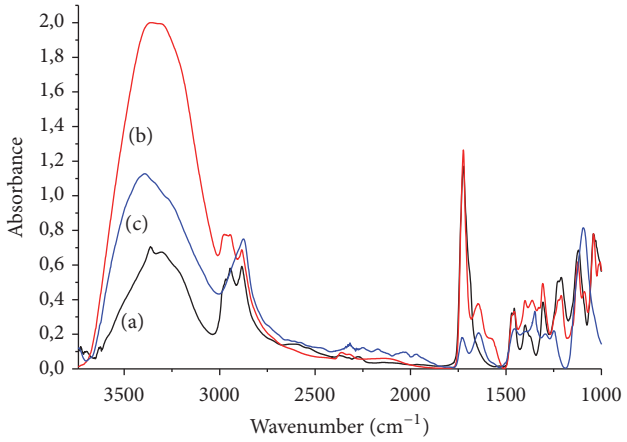

Figure 7: FT-IR spectra of HBPO BH20 (a), CoNPs (12 : 1) (b), and CoNPs (16 : 1) (c).

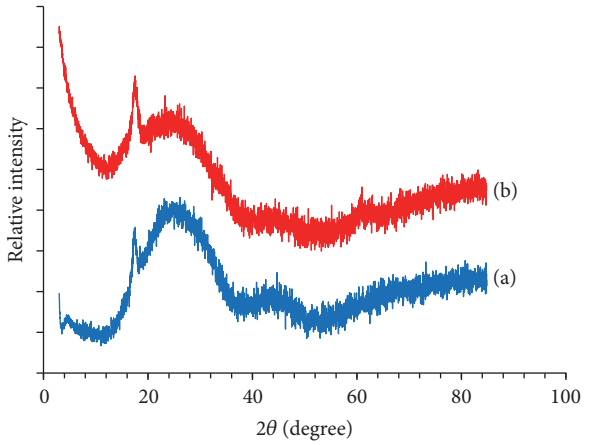

Figure 8: XRD powder pattern of CoNPs (12 : 1) (a) and CoNPs (16 : 1) (b).

at 3356 cm^{-1} could be associated with the increasing number of hydrogen bonds. Moreover during the synthesis of CoNPs (16 : 1) a partial destruction of ester bonds took place. That fact was indicated by a decrease in signal strength at 1720, 1305, 1220, and 1120 cm^{-1} and increase of peak intensity at 2878 cm^{-1} [35, 43].

XRD pattern indicated the amorphous structure of products. The broadening of the diffraction peaks of CoNPs (12 : 1) (Figure 8(a)) and CoNPs (16 : 1) (Figure 8(b)) suggests the presence of small particles [28, 29]. The diffraction peaks at 2θ = 19.4° and 21° refer to reflections of the HBPO matrix, and a maximum at 47.9° and a wide reflex with a maximum at 79.6^0 can be attributed to the metallic Co°, in which the alternating microdomains with cubic and hexagonal packings were observed.

The magnetic curves field dependence of magnetization of CoNPs (12 : 1) was measured at 5, 10, 50, 100, 200, and 360 K (Figure 9). The magnetization curves of the sample CoNPs (12 : 1), measured at 5, 10, and 50 K, had visible hysteresis loops [2, 3]. The loops are closed and symmetrical versus the origin of the coordinate system form. The magnetization under field of 10 kOe was 5.87 emug^{-1}. The remanence magnetization

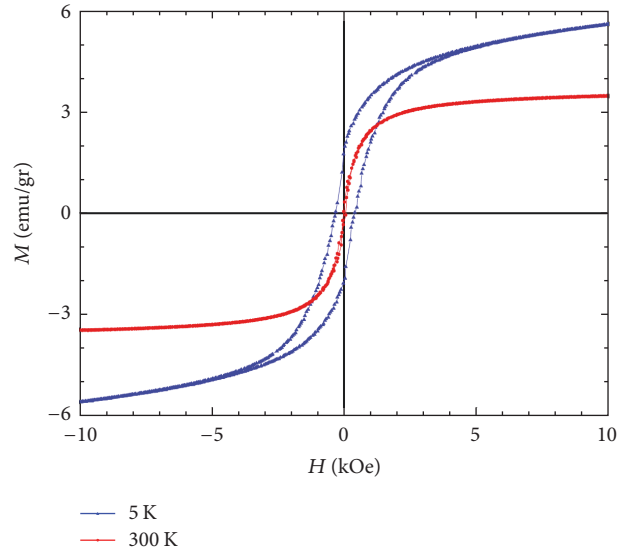

Figure 9: Hysteresis loops obtained at 5 K and 300 K for CoNPs (12 : 1).

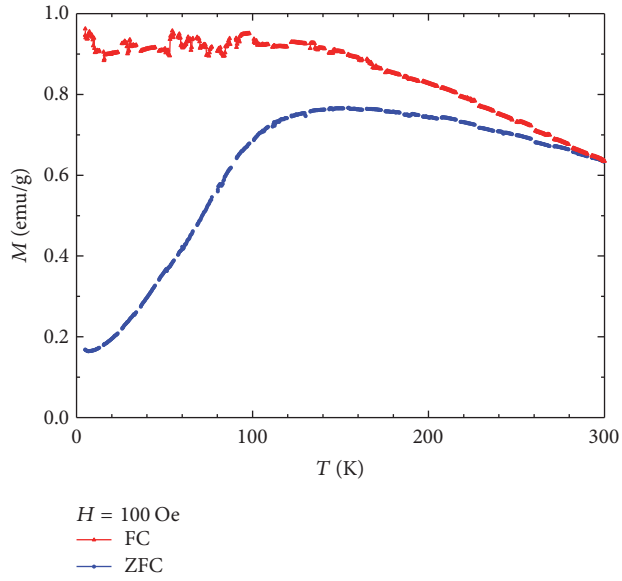

Figure 10: ZFC–FC curves measured in an applied field of 100 Oe for CoNPs (12 : 1).

value (Mr) was 2.06 emug^{-1}, and the coercivity was 323 Oe. The magnetization curves showed neither hysteresis nor coercivity. The saturated magnetization values (Ms) measured at 100, 200, and 300 K were 4.56, 4.16, and 3.62 emug^{-1}, respectively.

The temperature dependence of the magnetization was measured under magnetic field of 100 Oe from 5 to 300 K using zero field-cooled (ZFC) and field-cooled (FC) procedure. This measurement allowed determining the blocking temperature of CoNPs. The obtained ZFC–FC curves of CoNPs (12 : 1) nanocomposite are displayed in Figure 10. Magnetization of CoNPs increased with the increase of the temperature that is shown at the ZFC curve. The wide peak was observed at 100–170 K with maximum at 140 K. The maximum temperature is called blocking temperature Tb. The thermal energy becomes comparable to the energy barrier of magnetic anisotropy for spin reorientation at blocking temperature.

Table 2: Hydrodynamic diameter (d_h) from NTA measurements of nanoparticles CoNPs in aqueous solution.

CoNPs	d_h, nm
CoNPs (8 : 1)	106 ± 15
CoNPs (10 : 1)	107 ± 20
CoNPs (12 : 1)	112 ± 10
CoNPs (16 : 1)	123 ± 18

At a temperature of 300 K discrepancy between the ZFC and FC curves was observed. A sufficiently high temperature, which characterizes the temperature of irreversible magnetic changes, is associated with a wide size distribution of nanoparticles in the sample and strong interaction between the particles [2].

The variations in size, determined by different methods, were due to the fact that these methods rely on different physical principles and/or detection methods. In addition, electron microscopy probes dry particles, that is, the metallic core only, whereas the NTA probe the hydrodynamic diameter which is always larger. The size predicted by TEM analysis was found to be smaller than predicted by NTA analysis.

According to the NTA method hydrodynamic diameter of CoNPs nanocomposite rose from 106 ± 15 to 123 ± 18 nm (Figure 11, Supplementary Figures S3, S4) with increase of molar ratio Co^{2+} : BH20; however it was smaller than the diameter of respective complex forms of Co_n(BH20) (Table 2, Supplementary Table S5).

The successful formation of CoNPs was first confirmed by TEM studies. Figure 12 shows the TEM micrographs and size distributions of CoNPs nanoparticles (12 : 1) obtained using HBPO BH20 as a stabilizer. The nanoparticles CoNPs (12 : 1) were approximately spherical, with size about 8.2 ± 3.4 nm. Particles have aggregated easily, probably because of the high mobility of the particles as well as the magnetic interaction between the particles.

4. Conclusions

Thus, for the first time the process of preorganization of Co^{2+} ions on the platform of a hyperbranched polyester polyol of the second generation was studied and the significant complex forms of Co_n(BH20) existing in an aqueous solution were determined. The cobalt nanoparticles were synthesized by the chemical reduction method in solution at various molar ratios of $CoCl_2$: HBPO. It is shown that an increase in the concentration of Co^{2+} ions in the polymer matrix at the preorganization stage leads to an increase in the proportion of oxide forms in the composition of the nanoparticles. CoNPs synthesized at the $CoCl_2$: HBPO molar ratio of 12 : 1 have possessed the highest stability. They had spherical shape; moreover, metallic nanoclusters of cobalt with a diameter of 8.2 ± 3.4 nm were in the polymer shell of the stabilizer.

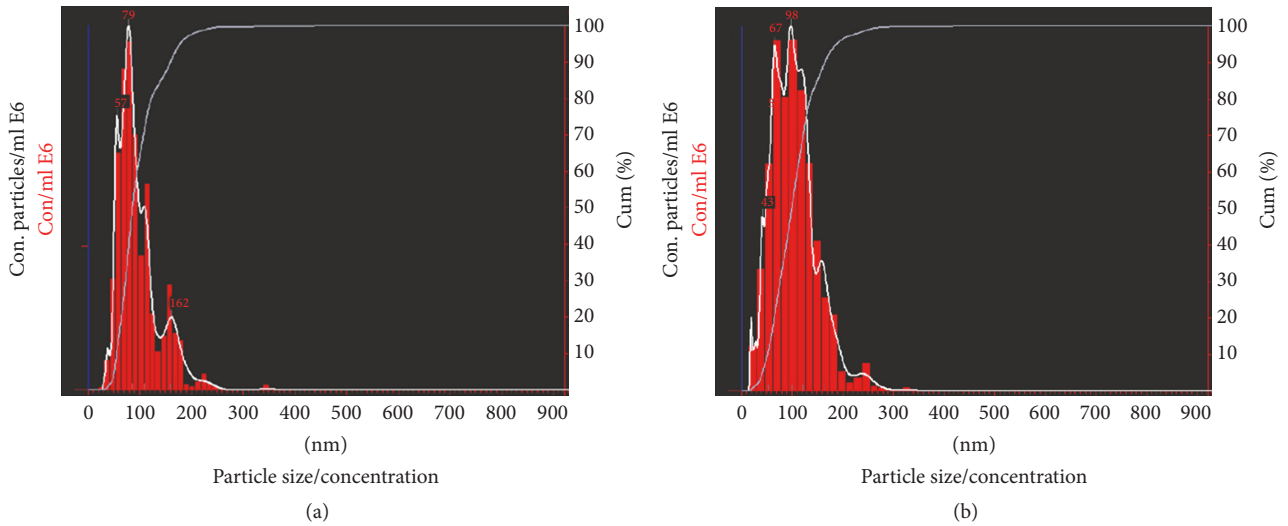

Figure 11: Concentration and size distribution from NTA measurements of CoNPs (8 : 1) (a) and CoNPs (12 : 1) (b) in aqueous solution.

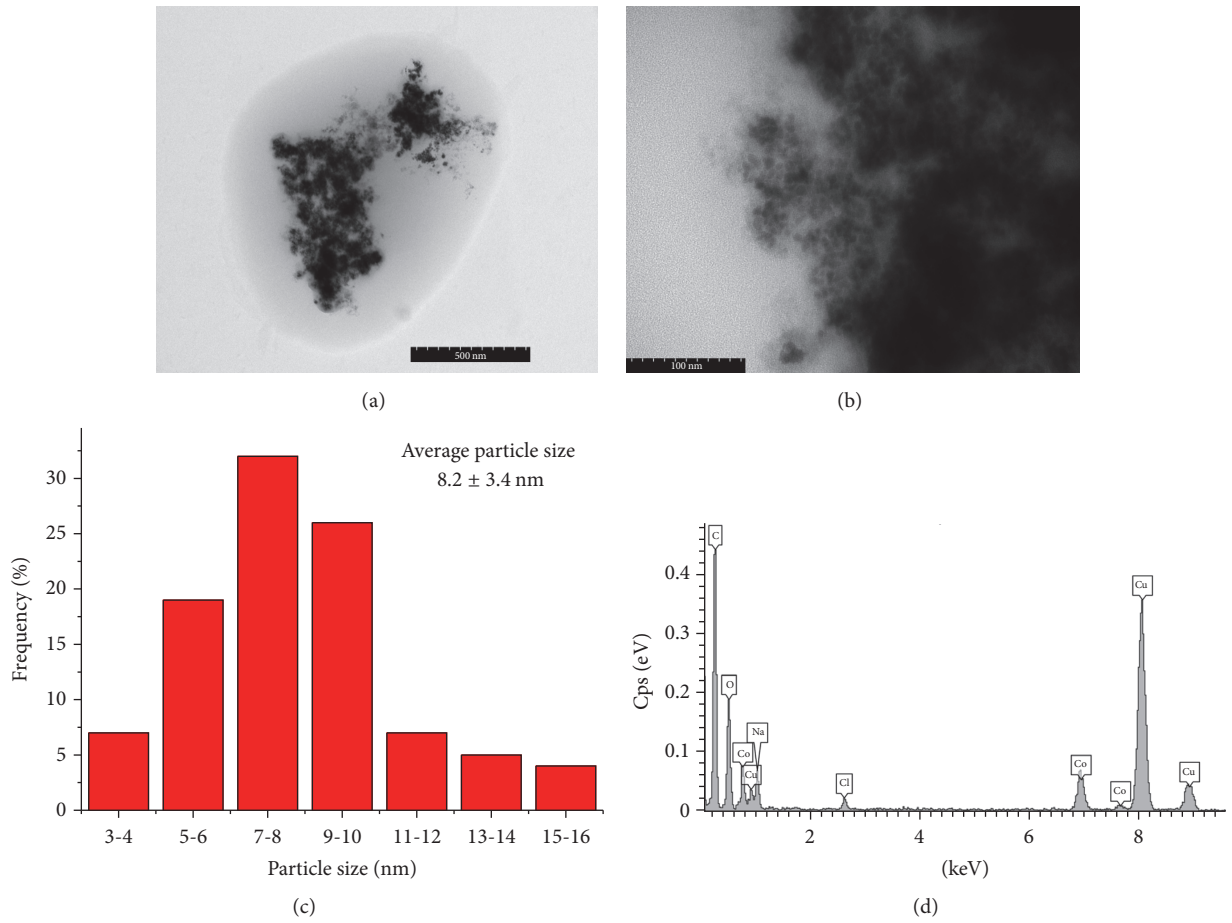

Figure 12: TEM images CoNPs (12 : 1) (a, b), corresponding particle-size distribution of CoNPs (c), and EDS spectrum (d) for the area corresponding to (a). The Cu signals come from TEM grids.

It has been proved that the polymer-composite nanoparticles Co/BH20 (12 : 1) exhibit magnetic properties, including superparamagnetic properties at room temperature, which will allow them to be used for further development of MRI diagnostic systems as well as targeted drug delivery system.

Conflicts of Interest

The authors O. I. Medvedeva, S. S. Kambulova, O. V. Bondar, A. R. Gataulina, N. A. Ulakhovich, A. V. Gerasimov, V. G. Evtugyn, I. F. Gilmutdinov, and M. P. Kutyreva declare that there are no conflicts of interest regarding the publication of this paper.

Acknowledgments

The magnetic measurements were carried out at the Federal Center of Shared Facilities of Kazan Federal University. Microscopy studies were carried out at the Interdisciplinary Center of Analytical Microscopy of Kazan Federal University. The work is performed according to the Russian Government Program of Competitive Growth of Kazan Federal University.

References

[1] L. Merhari, *Hybrid Nanocomposites for Nanotechnology: Electronic, Optical, Magnetic and Biomedical Applications*, Springer, Boston, MA, USA, 2009.

[2] S. Gubin, *Magnetic Nanoparticles*, WILEY-VCH Verlag GmbH & Co. KGaA, 2009.

[3] Q. A. Pankhurst, J. Connolly, S. K. Jones, and J. Dobson, "Applications of magnetic nanoparticles in biomedicine," *Journal of Physics D: Applied Physics*, vol. 36, no. 13, pp. R167–R181, 2003.

[4] W. H. Suh, Y. H. Suh, and G. D. Stucky, *Nano Today*, vol. 4, pp. 27–36, 2009.

[5] T. K. Indira and R. K. Lakshmi, *International Journal of Pharmaceutical Sciences and Nanotechnology*, vol. 3, pp. 1035–1042, 2010.

[6] P. P. Waifalkar, S. B. Parit, A. D. Chougale, S. C. Sahoo, P. S. Patil, and P. B. Patil, "Immobilization of invertase on chitosan coated γ-Fe2O3 magnetic nanoparticles to facilitate magnetic separation," *Journal of Colloid and Interface Science*, vol. 482, pp. 159–164, 2016.

[7] J. Chomoucka, J. Drbohlavova, D. Huska, V. Adam, R. Kizek, and J. Hubalek, "Magnetic nanoparticles and targeted drug delivering," *Pharmacological Research*, vol. 62, no. 2, pp. 144–149, 2010.

[8] A. M. Nyström and B. Fadeel, "Safety assessment of nanomaterials: implications for nanomedicine," *Journal of Controlled Release*, vol. 161, no. 2, pp. 403–408, 2012.

[9] P. Padmanabhan, A. Kumar, S. Kumar, R. K. Chaudhary, and B. Gulyás, "Nanoparticles in practice for molecular-imaging applications: An overview," *Acta Biomaterialia*, vol. 41, pp. 1–16, 2016.

[10] R. S. Chaughule, S. Purushotham, and R. V. Ramanujan, "Magnetic Nanoparticles as Contrast Agents for Magnetic Resonance Imaging," *Proceedings of the National Academy of Sciences, India Section A: Physical Sciences*, vol. 82, no. 3, pp. 257–268, 2012.

[11] J. Verma, S. Lal, and C. J. F. van Noorden, "Nanoparticles for hyperthermic therapy: synthesis strategies and applications in glioblastoma," *International Journal of Nanomedicine*, vol. 9, no. 1, pp. 2863–2877, 2014.

[12] N. Shatrova, A. Yudin, V. Levina et al., "Elaboration, characterization and magnetic properties of cobalt nanoparticles synthesized by ultrasonic spray pyrolysis followed by hydrogen reduction," *Materials Research Bulletin*, vol. 86, pp. 80–87, 2017.

[13] H. Shokrollahi and L. Avazpour, "Influence of intrinsic parameters on the particle size of magnetic spinel nanoparticles synthesized by wet chemical methods," *Particuology*, vol. 26, pp. 32–39, 2016.

[14] S. Gopinath, K. Sivakumar, B. Karthikeyen, C. Ragupathi, and R. Sundaram, "Structural, morphological, optical and magnetic properties of Co3O4 nanoparticles prepared by conventional method," *Physica E: Low-Dimensional Systems and Nanostructures*, vol. 81, pp. 66–70, 2016.

[15] L. Pan, L. Li, and C. Yo, "Synthesis of hexagonal Co_3O_4 and Ag/Co_3O_4 composite nanosheets and their electrocatalytic performances," *Journal of Cluster Science*, vol. 24, no. 4, pp. 1001–1010, 2013.

[16] H. T. Yang, Y. K. Su, C. M. Shen, T. Z. Yang, and H. J. Gao, "Synthesis and magnetic properties of ε-cobalt nanoparticles," *Surface and Interface Analysis*, vol. 36, no. 2, pp. 155–160, 2004.

[17] Y. Dong, G. Wang, P. Jiang, A. Zhang, L. Yue, and X. Zhang, "Catalytic ozonation of phenol in aqueous solution by Co3O4 nanoparticles," *Bulletin of the Korean Chemical Society*, vol. 31, no. 10, pp. 2830–2834, 2010.

[18] Y. Liang, Y. Li, H. Wang et al., "Co_3O_4 nanocrystals on graphene as a synergistic catalyst for oxygen reduction reaction," *Nature Materials*, vol. 10, no. 10, pp. 780–786, 2011.

[19] F. Moro, S. V. Tang, F. Tuna, and E. Lester, "Detection of para–antiferromagnetic transition in $Bi_2Fe_4O_9$ powders by means of microwave absorption measurements," *Journal of Magnetism and Magnetic Materials*, vol. 348, pp. 17–21, 2013.

[20] J. Park, X. Shen, and G. Wang, "Solvothermal synthesis and gas-sensing performance of Co_3O_4 hollow nanospheres," *Sensors and Actuators B: Chemical*, vol. 136, no. 2, pp. 494–498, 2009.

[21] Y. Xu, C. Wang, Y. Sun, G. Zhang, and D. Gao, "Fabrication and characterization of nearly monodisperse Co_3O_4 nanospheres," *Materials Letters*, vol. 64, no. 11, pp. 1275–1278, 2010.

[22] H. Bönnemann, W. Brijoux, R. Brinkmann et al., "A size-selective synthesis of air stable colloidal magnetic cobalt nanoparticles," *Inorganica Chimica Acta*, vol. 350, pp. 617–624, 2003.

[23] M. Edrissi and A. R. Keshavarz, "Synthesis of cobalt chromite nanoparticles by thermolysis of mixed Cr^{3+} and Co^{2+} chelates of 2-mercaptopyridin N-Oxide," *Nano-Micro Letters*, vol. 4, no. 2, pp. 83–89, 2012.

[24] S. A. Novopashin, M. A. Serebryakova, and S. Y. Khmel, "Methods of magnetic fluid synthesis (review)," *Thermophysics and Aeromechanics*, vol. 22, no. 4, pp. 397–412, 2015.

[25] S. A. Usami, "Synthesis and Characterization of Cobalt Nanoparticles Using Hydrazine and Citric Acid," *Journal of Nanotechnology*, vol. 2014, Article ID 525193, 6 pages, 2014.

[26] J. P. Rao, P. Gruenberg, and K. E. Geckeler, "Magnetic zerovalent metal polymer nanoparticles: Current trends, scope, and perspectives," *Progress in Polymer Science*, vol. 40, pp. 138–147, 2015.

[27] M. Zhao, L. Sun, and R. M. Crooks, "Preparation of Cu nanoclusters within dendrimer templates," *Journal of the American Chemical Society*, vol. 120, no. 19, pp. 4877-4878, 1998.

[28] H. Kavas, Z. Durmus, E. Tanriverdi, M. Şenel, H. Sozeri, and A. Baykal, "Fabrication and characterization of dendrimer-encapsulated monometallic Co nanoparticles," *Journal of Alloys and Compounds*, vol. 509, no. 17, pp. 5341–5348, 2011.

[29] H.-X. Wu, C.-X. Zhang, L. Jin, H. Yang, and S.-P. Yang, "Preparation and magnetic properties of cobalt nanoparticles with dendrimers as templates," *Materials Chemistry and Physics*, vol. 121, no. 1-2, pp. 342–348, 2010.

[30] K. Aranishi, Q.-L. Zhu, and Q. Xu, "Dendrimer-Encapsulated Cobalt Nanoparticles as High-Performance Catalysts for the Hydrolysis of Ammonia Borane," *Chem. Cat. Chem*, vol. 6, no. 5, pp. 1375–1379, 2014.

[31] K. InoueK, *Prog. Polym. Sci*, vol. 25, pp. 453–571, 2000.

[32] B. I. Voit and A. Lederer, "Hyperbranched and highly branched polymer architectures-synthetic strategies and major characterization aspects," *Chemical Reviews*, vol. 109, no. 11, pp. 5924–5973, 2009.

[33] E. Zagar and J. Grdadolnik, "An infrared spectroscopic study of H-bond network in hyperbranched polyester polyol," *Journal of Molecular Structure*, vol. 658, no. 3, pp. 143–152, 2003.

[34] E. Zagar and M. Zigon, "Aliphatic hyperbranched polyesters based on 2,2-bis(methylol)propionic acid—Determination of structure, solution and bulk properties," *Progress in Polymer Science*, vol. 36, no. 1, pp. 53–88, 2011.

[35] R. Arote, T.-H. Kim, Y.-K. Hwang et al., "A biodegradable poly(ester amine) based on polycaprolactone and polyethylenimine as a gene carrier," *Biomaterials*, vol. 28, pp. 735–744, 2007.

[36] L. M. Bronstein and Z. B. Shifrina, "Nanoparticles in dendrimers: From synthesis to application," *Nanotechnologies in Russia*, vol. 4, no. 9-10, pp. 576–608, 2009.

[37] R. A. Ahmadi, F. Hasanvand, G. Bruno, H. A. Rudbari, S. Amani, and J. Beilstein, "Synthesis, Spectroscopy, and Magnetic Characterization of Copper(II) and Cobalt(II) Complexes with 2-Amino-5-bromopyridine as Ligand," *ISRN Inorganic Chemistry*, vol. 2013, Article ID 426712, 7 pages, 2013.

[38] P. Petkova and V. Nedkov, "Behavior of Co2+ cations in the aqueous and alcoholic solution of CoCl2.6H2O," *Acta Physica Polonica A*, vol. 123, no. 2, pp. 207-208, 2013.

[39] Ö. Metin and S. Özkar, "Water soluble nickel(0) and cobalt(0) nanoclusters stabilized by poly(4-styrenesulfonic acid-co-maleic acid): Highly active, durable and cost effective catalysts in hydrogen generation from the hydrolysis of ammonia borane," *International Journal of Hydrogen Energy*, vol. 36, no. 2, pp. 1424–1432, 2011.

[40] S. Karahan and S. Özkar, "Poly(4-styrenesulfonic acid-co-maleic acid) stabilized cobalt(0) nanoparticles: A cost-effective and magnetically recoverable catalyst in hydrogen generation from the hydrolysis of hydrazine borane," *International Journal of Hydrogen Energy*, vol. 40, no. 5, pp. 2255–2265, 2015.

[41] L. M. Alrehaily, J. M. Joseph, M. C. Biesinger, D. A. Guzonas, and J. C. Wren, "Gamma-radiolysis-assisted cobalt oxide nanoparticle formation," *Physical Chemistry Chemical Physics*, vol. 15, no. 3, pp. 1014–1024, 2013.

[42] M. Yarestani, A. D. Khalaji, A. Rohani, and D. Das, "Hydrothermal synthesis of cobalt oxide nanoparticles: Its optical and magnetic properties," *Journal of Sciences, Islamic Republic of Iran*, vol. 25, no. 4, pp. 339–343, 2014.

[43] F. A. Miller and C. H. Wilkins, "Infrared spectra and characteristic frequencies of inorganic ions: their use in qualitative analysis," *Analytical Chemistry*, vol. 24, no. 8, pp. 1253–1294, 1952.